Silica−Polyamine-Based Carbon Composite Adsorbents as Media for Effective Hydrogen Sulfide Adsorption/Oxidation

Teresa J. Bandosz,*,† Mykola Seredych,† Jesse Allen,‡ Jessica Wood,‡ and Edward Rosenberg*,‡

Department of Chemistry, The City College of New York, 138th Street and Convent Avenue, New York, New York 10031, and Department of Chemistry, University of Montana, Missoula, Montana 59812

Received December 15, 2006. Revised Manuscript Received March 7, 2007

New silica−carbon adsorbents were prepared by pyrolysis of silica−polyamine composites at 600 °C. The heat treatment was expected to activate nitrogen for effective hydrogen sulfide oxidation. Moreover, the same pyrolysis treatment was applied on silica−polyamine adsorbents previously used to remove copper ions for aqueous solution. The performance of these materials as H_2S adsorbents was tested using a home-developed dynamic breakthrough test. Samples from before and after the adsorption process were characterized by adsorption of nitrogen, surface pH, thermal analysis, elemental analysis, FTIR, optical microscopy, and solid-state CPMAS ^{13}C NMR. Differences in the performance were linked to the surface properties such as content of nitrogen, content of copper, surface acidity/basicity, and porous structure. It was found that the capacity for hydrogen sulfide removal/selectivity for oxidation to sulfur depends on the granulation of the silica matrix, the kind of polymer used for grafting, surface basicity, and porosity. Thermal transformation of the polymer causes the formation of new highly dispersed catalytic centers with active nitrogen atoms. The silica matrix also provides pore space for the storage of oxidation products, mainly elemental sulfur.

1. Introduction

The search for new sources of energy coming from biomass results in an increased demand for effective removal of pollutants. Examples of these pollutants are sulfur-containing compounds formed during anaerobic digestion of an organic matter. Such compounds (e.g., hydrogen sulfide, dimethyl sulfide, thiophene, benzothiophenes), besides having detrimental (acid rain) and toxic effects on the environment, are well-known sources of poisoning for reforming catalysts. The latter has become a problem when the gases containing sulfur even at the parts per billion levels are used as a source of hydrogen for fuel-cell operation.

Removal of sulfur-containing gases is carried out either at ambient or elevated temperatures. Although the former is applied for desulfurization of air,[1,2] natural gas,[3−8] or biogas,[9,10] the latter is important in the case of syngas.[11] Under ambient conditions, activated carbons with various surface modifications are used,[1] whereas at high temperatures (>400 °C), oxide- or ceramic-based membranes were found to be effective media.[11,12]

The advantage of activated carbons over oxide-based adsorbents is in their high surface area and pore volume, where huge amounts of oxidation products can be stored, and in their numerous possibilities for making surface chemistry modifications.[13] Their disadvantage lies in surface instability at high temperatures and strong adsorption forces, which make their in situ regeneration problematic.[1,14,15]

One of the ways to increase an activated carbon's capacity for gas-phase desulfurization is by shifting its surface pH toward highly basic values, which promotes dissociation of hydrogen sulfide or methyl mercaptanes.[1,16] This is usually done via impregnation with caustics[1,18,19] or alkali metal

* To whom correspondence should be addressed. Tel: (212) 650-6017 (T.B.); (406) 243-2592 (E.R.). Fax: (212) 650-6107 (T.B.); (406) 243-4227 (E.R.). E-mail: tbandosz@ccny.cuny.edu (T.B.); edward.rosenberg@mso.umt.edu (E.R.).
† City University of New York.
‡ University of Montana.

(1) Bandosz, T. J. *J. Colloid Interface Sci.* **2002**, *246*, 1.
(2) Bagreev, A.; Bandosz, T. J. *Ind. Chem. Eng. Res.* **2005**, *44*, 530.
(3) Coskun, I.; Tollefson, E. L. *Can. J. Chem. Eng.* **1986**, *58*, 72.
(4) Ghosh, T. K.; Tollefson, E. L. *Can. J. Chem. Eng.* **1986**, *64*, 960.
(5) Ghosh, T. K.; Tollefson, E. L. *Can. J. Chem. Eng.* **1986**, *64*, 969.
(6) Dalai, A. K.; Majumadar, M.; Chowdhury, A.; Tollefson, E. L. *Can. J. Chem. Eng.* **1993**, *71*, 75.
(7) Yang, A.; Tollefson, E. L.; Dalai, A. K. *Can. J. Chem. Eng.* **1998**, *76*, 76.
(8) Dalai, A. K.; Tollefson, E. L. *Can. J. Chem. Eng.* **1986**, *76*, 902.
(9) Bagreev, A.; Katikaneni, S.; Parab, S.; Bandosz, T. J. *Catal. Today* **2005**, *99*, 329.
(10) Seredych, M.; Bandosz, T. J. *Ind. Chem. Eng. Res.* **2006**, *45*, 3658.
(11) Flytzani-Stephanopoulos, M.; Sakbodin, M.; Wang, Z. *Science* **2006**, *312*, 1508.
(12) Sirling, D. *The Sulfur Problem: Cleaning up Industrial Feedstocks*; Royal Commonwealth Society: Cambridge, U.K., 2000.
(13) Bandosz, T. J.; Ania, C. O. Surface Chemistry of Activated Carbons and its Characterization. In *Activated Carbon Surfaces in Environmental Remediation*; Bandosz, T. J., Ed.; Elsevier: Amsterdam, U.K., 2006; pp 159−231.
(14) Bansal, R. C.; Donnet, J. B.; Stoeckli, F. *Active Carbon*; Marcel Dekker: New York, 1988.
(15) Adil, F.; Bagreev, A.; Bandosz, T. J. *Ind. Eng. Chem. Res.* **2000**, *39*, 2439.
(16) Bandosz, T. J. Desulfurization on Activated Carbons. In *Activated Carbon Surfaces in Environmental Remediation*; Bandosz, T. J., Ed.; Elsevier: Amsterdam, 2006; pp 231−293.
(17) Bashkova, S.; Bagreev, A.; Bandosz, T. J. *Ind. Chem. Eng. Res.* **2002**, *41*, 4346.
(18) Bagreev, A.; Bandosz, T. J. *Ind. Eng. Chem. Res.* **2002**, *41*, 672.
(19) Adib, F.; Bagreev, A.; Bandosz, T. J. *Environ. Sci. Technol.* **2000**, *34*, 686.

10.1021/cm062984i CCC: $37.00
Published on Web 04/20/2007

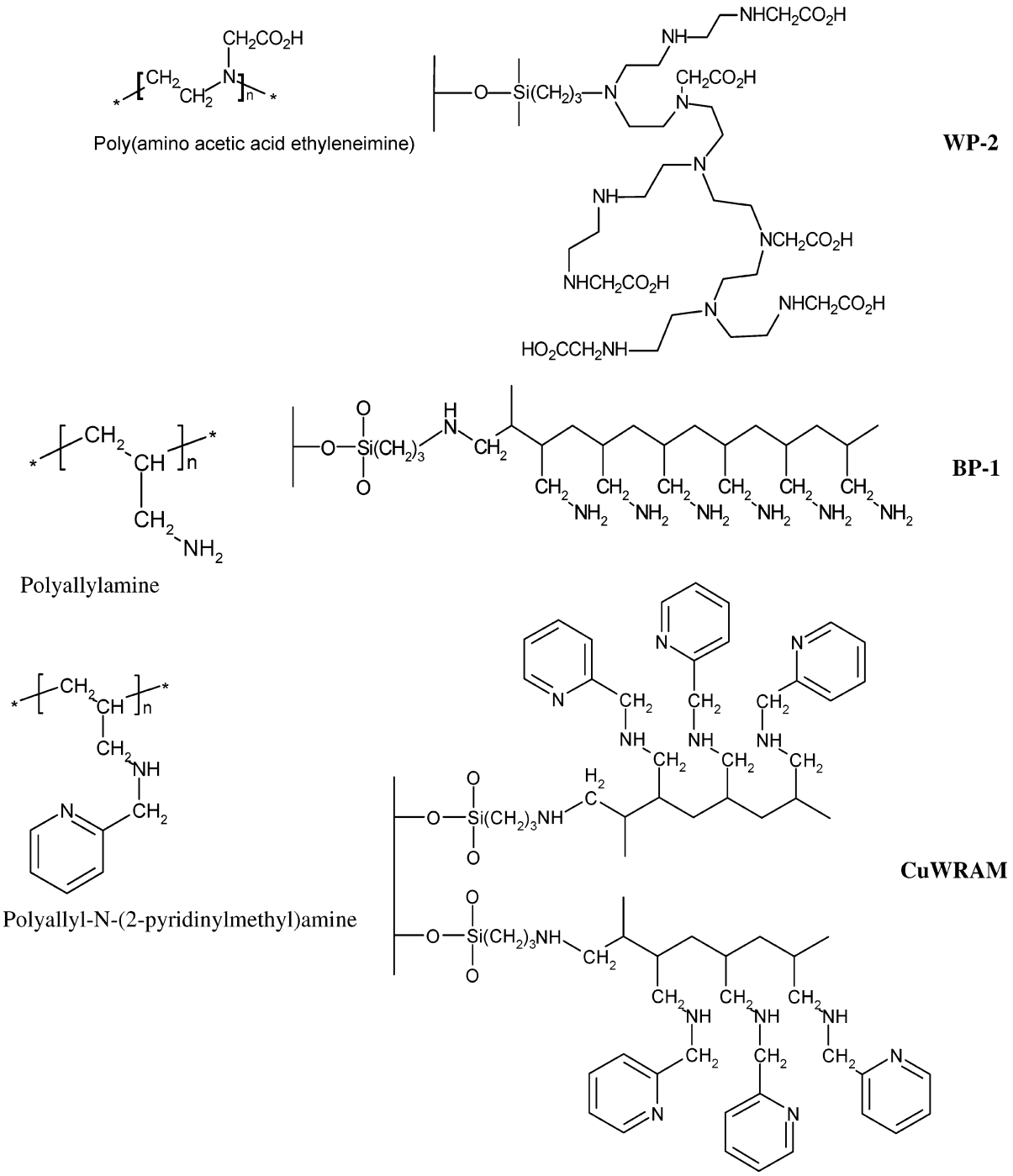

Figure 1. Organic polyamines grafted to the silica surface.

carbonates.[20,21] The overall surface pH can be also changed when alkaline earth oxides are added as catalysts[22] or basic nitrogen-containing species are introduced onto the surface.[23,24] The latter process is done via impregnation of a carbon surface with nitrogen-containing organic compounds followed by their high-temperature conversion to pyridinyl or quaternary nitrogen.[25] These nitrogen centers were found to be an important factor for activating oxygen and thus enhancing oxidation of reduced sulfur compounds.[25−27] Another species that was found to play a role in oxygen activation is copper in a highly dispersed state on the carbon surface.[28] It significantly increases the efficiency of desulfurization adsorbents and its presence increases selectivity for elemental sulfur as an oxidation product.

(20) Przepiorski, J.; Oya, A. *J. Mater. Sci. Lett.* **1998**, *17*, 679.
(21) Przepiorski, J.; Abe, Y.; Yoshida, S.; Oya, A. *J. Mater. Sci. Lett.* **1997**, *16*, 1312.
(22) Graham, J. Activated carbon for odor control and method for making some. U.S. Patent 6 858 192, 2005.
(23) Hayden, R. A. Process for making catalytic carbon. U.S. Patent 5 444 031, 1995.
(24) Adib, F.; Bagreev, A.; Bandosz, T. J. *Langmuir* **2000**, *16*, 1980.
(25) Strohr, B.; Boehm, H. P.; Schlogl, R. *Carbon* **1991**, *26*, 707.
(26) Biniak, S.; Szymanski, G.; Siedlewski, J.; Swiatkowski, A. *Carbon* **1997**, *35*, 1799.
(27) Bagreev, A.; Menendez, J. A.; Dukhno, I.; Tarasenko, Y.; Bandosz, T. J. *Carbon* **2004**, *42*, 469.
(28) Nguyen-Thanh, D.; Bandosz, T. J. *Carbon* **2005**, *43*, 359.

Table 1. Name of Adsorbents (after Pyrolysis "C" is Added in Front of the Initial Sample Name), Nitrogen-Containing Polymer, Granulation, and Yield

sample	N-containing polymer	granulation (μm)	yield (%)
CBP-1 (from BP-1)	polyallylamine linear (MW=1500)	150−250	64
CBP-1-Cu	above + Cu		68
CWP-2A (from WP-2A)	polyethyleneimine branched (MW=1200) + $CH_2ClCOOH$	150−250	66
CWP-2A-Cu	above + Cu	150−250	69
CWP-2B (from WP-2B)	polyethyleneimine branched (MW=1200) + $CH_2ClCOOH$	250−540	65
CWP-2B-Cu	above + Cu	250−540	78
CWram (from CuWRAM)	polyallylamine linear (MW=1500) + 2 chloromethyl pyridne	250−500	61
CWram-Cu	above + Cu	250−500	66

Table 2. Copper, Carbon, Hydrogen, and Nitrogen Contents (%) after Pyrolysis and Carbon, Hydrogen, and Nitrogen Contents of Selected Composites prior to Pyrolysis (%)

After Pyrolysis					
sample	C	H	N	N/C	Cu
CBP-1	5.07	0.85	<0.10	0.02	
CBP-1-Cu	9.61	0.74	0.47	0.05	4.4
CWP-2A	8.01	0.78	1.52	0.19	
CWP-2A-Cu	7.83	1.60	1.57	0.20	3.4
CWP-2B	3.60	0.59	0.48	0.13	
CWP-2B-Cu	3.82	0.41	0.44	0.11	3.4
CWram	16.9	1.26	2.29	0.13	
CWram-Cu	18.2	1.56	2.54	0.14	5.7

Prior to Pyrolysis				
sample	C	H	N	N/C
BP-1	13.5	2.96	3.85	0.27
WP-2A	14.98	3.02	4.32	0.29
WP-2B	11.59	3.07	2.92	0.25
CuWRAM	16.58	2.29	4.47	0.27

The objective of this paper is to evaluate the suitability of silica−polyamine-based composite adsorbents as hydrogen sulfide removal media. These materials contain a thin carbon layer with incorporated nitrogen functionalities, which can activate oxygen.[25] Moreover, the silica matrix provides storage space in large pores (mesopores, mostly in the range of 10−30 nm), which might be more effective than the small pores of activated carbons.[29,30] Because these silica polyamine composites are already designed for use on the industrial scale as adsorbents of copper from mine waters,[31] a new window of opportunity for an inexpensive way of surface modification via incorporation of a catalytically active metal can also be explored. The results are analyzed from the point of view of the importance of the surface features for oxidation of hydrogen sulfide to elemental sulfur. Another important aspect of these new materials lies in their greater thermal stability compared with that of activated carbons and the large pores in which there are hardly any diffusion limitations. The former may indicate an application of this kind of materials for high-temperature desulfurization of syngas.

2. Experimental Section

2.1. Materials. Adsorbents were prepared from silica−polyamine composites BP-1, WP-2(A), WP-2(B), and CuWRAM.[31] Schematic structures of the composites are shown in Figure 1. The composites were prepared by published literature procedures.[31] To produce adsorbents containing copper, we exposed the samples to a cation exchange process with a 3 g/L solution of $CuSO_4$ (10 g of adsorbents and 100 mL of solution). In all cases, the pyrolysis was done in a horizontal furnace under a nitrogen atmosphere with a heating rate 10°/min. The final pyrolysis temperature was 600 °C with a 0.5 h holding time. The names of adsorbents and their yields are collected in Table 1. After exposure to hydrogen sulfide and exhaustion, a letter E is added to the name of the adsorbent.

2.2. Methods. *Evaluation of H_2S Sorption Capacity.* A custom-designed dynamic test was used to evaluate the performance of adsorbents for H_2S adsorption from gas streams as described elsewhere.[1] Adsorbent samples were packed into a glass column (length 370 mm, internal diameter 9 mm, bed volume 6 cm^3) and pre-humidified with moist air (relative humidity 80% at 25 °C) for 2 h. The amount of water adsorbed was estimated from the increase in the sample weight. Moist air (relative humidity 70% at 25 °C) containing 0.3% (3000 ppm) of H_2S was passed through the column of the adsorbent at 0.5 L/min. The flow rate was controlled using Cole Palmer flow meters. The breakthrough of H_2S was monitored using electrochemical sensors. The test was stopped at the breakthrough concentration of 100 ppm. The adsorption capacities of each adsorbent in terms of milligrams of hydrogen sulfide per gram of adsorbent were calculated by integration of the area above the breakthrough curves and from the H_2S concentration in the inlet gas, flow rate, breakthrough time, and mass of sorbent. For each sample, the test was repeated at least twice.

To check the influence of water, the best-performing samples were exposed to H_2S adsorption from moist air without pre-humidification. Such samples are referred to with an additional letter D.

Characterization of the Pore Structure of Adsorbents. Sorption of nitrogen at its boiling point was carried out using ASAP 2010 (Micromeritics) on the materials obtained. Before the experiments, the samples were outgassed at 120 °C to a constant vacuum (1×10^{-4} Torr). From the isotherms, the surface areas (BET method), total pore volumes V_t (from the last point of the isotherm at a relative pressure equal to 0.99), volumes of micropores V_{mic}, mesopore volume V_{mes}, and pore size distributions (PSD) were calculated.[14] The PSDs were calculated using density functional theory, DFT.[32,33]

pH. The pH of an adsorbent was measured in a suspension and provided information about the acidity and basicity of the carbon surface. A sample of 0.4 g of the dry carbonized composite powder was added to 20 mL of distilled water and the suspension was stirred overnight to reach equilibrium. Then the pH of the suspension was measured.

Thermal Analysis. Thermal analysis was carried out using a TA Instruments Thermal Analyzer. The instrument settings were as

(29) Bandosz, T. J.; Block, K. *Environ. Sci. Technol.* **2006**, *40*, 3378.
(30) Bandosz, T. J.; Block, K. *Ind. Chem. Eng. Res.* **2006**, *45*, 3666.
(31) (a) Rosenberg, E.; Pang, D. System for extracting soluble heavy metals from liquid solution. U.S. Patent 5 695 882, 1997. (b) Rosenberg, E.; Pang, D. System for extracting soluble heavy metals from liquid solutions. U.S. Patent 5 997 748, 1999. (c) Rosenberg, E.; Fischer, R. U.S. Patent 6 576 303, 2003. (d) Hughes, M.; Nielsen, D.; Rosenberg, E.; Gobetto, R.; Viale, A.; Burton, S. D. *Ind. Eng. and Chem. Res.* **2006**, *45*, 6538.
(32) Lastoskie, Ch. M.; Gubbins, K. E.; Quirke, N. *J. Phys. Chem.* **1993**, *97*, 4786.
(33) Olivier, J. P. *J. Porous Mater.* **1995**, *2*, 9.

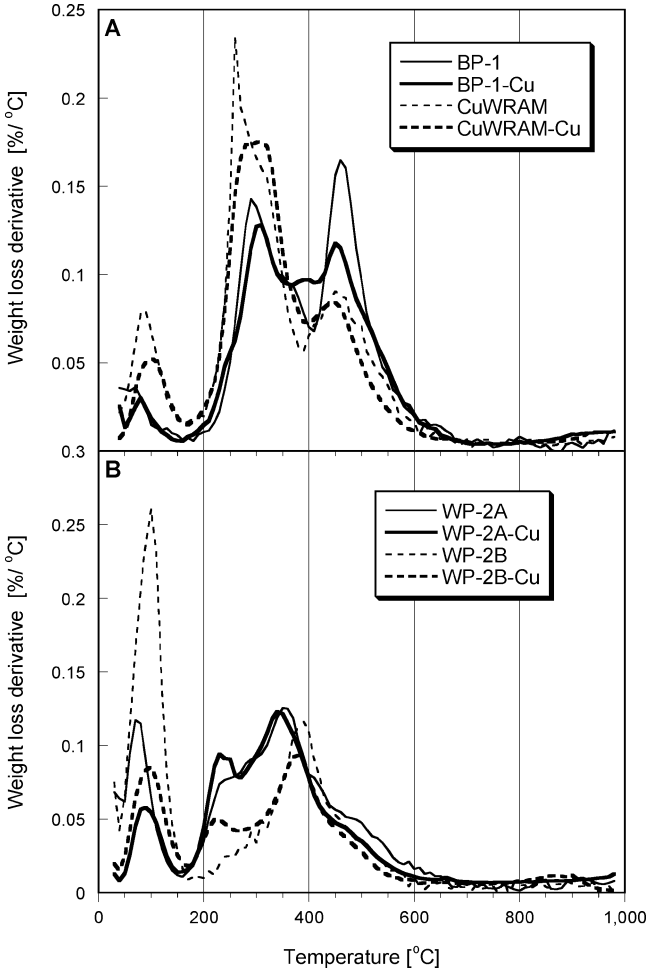

Figure 2. DTG curves in nitrogen for BP-1 and CuWRAM series of samples (A) and WP-2 series of samples (B).

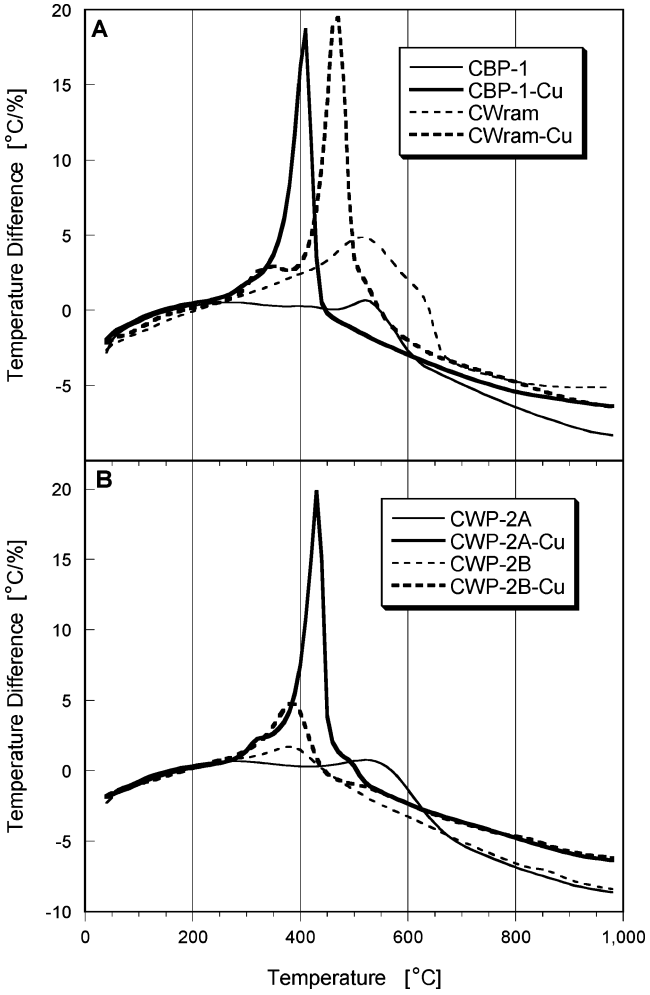

Figure 3. DTA curves in air for CBP-1 and CWram series of samples (A) and CWP-2 series of samples (B).

follows: heating rate of 10 °C/min and a nitrogen atmosphere with a 100 mL/min flow rate. For each measurement, about 25 mg of an adsorbent sample was used. Differential thermogravimetric curves (DTG) were chosen for analysis.

Elemental Analysis. Carbon, hydrogen, and nitrogen content were estimated by Schwarzkopf Microanalytical Laboratory, Woodside, NY. Copper content was calculated on the basis of the differences in concentration of copper solution before and after the ion-exchange process. The concentration was evaluated using Smart-Spectro at the wavelength of 410 nm.

Optical Microscopy. Optical microscopy images were obtained on a Nikon microscope using 5× and 2× magnifications.

FT-IR. FT-IR spectra were obtained on a Thermo-Nicolet 633 spectrophotometer as KBr pellets.

CPMAS ^{13}C NMR. CPMAS ^{13}C NMR were obtained at 125 MHz on a Varian 500 MHz instrument using 4 mm rotor with a spin speed of 7500 rpm.

3. Results and Discussion

The DTG curves for nitrogen for the initial materials are collected in Figure 2. Peaks represent mass loss due to the decomposition of organic matter and dehydroxylation of silica. For the BP-1 and CuWRAM series of samples (Figure 2A), the peaks are found at about 100 °C, between 200 and 400 °C, and between 400 and 600 °C. At temperatures higher than 600 °C, no major mass loss occurs, which was the rationale for choosing this temperature as the final pyrolysis temperature for our samples. Because these two samples have the same main polymer, polyallyamine (Table 1), we assign the peak between 200 and 600 °C to decomposition of the polymer manifested by its loss of hydrogen (likely in the form of hydrocarbons) and amine groups as NH_3. The latter likely decomposes at lower temperature.[34] This decomposition does not mean that nitrogen is totally removed from the sample. It can still be incorporated in various arrangements, as amine, pyridinyl, or quaternary nitrogen.[25] Differences in intensities of the peaks are related to differences in the incorporation of polymer onto the silica. As shown in Table 1, in the case of CuWRAM, picolylamine was also present in the system. Addition of copper decreases the mass loss, which might be related to the "dilution effect" of copper added to the mass of the sample. On the other hand, it can stabilize a carbon phase via chelation, and catalyze the graphitization process.

In the case of the WP-2 series of samples, the decomposition of the polymer occurs in the same temperature range (200−600 °C); however, the peaks are less intense (Figure 2B). It is interesting that the composite obtained from silica with larger particle sizes is thermally more stable and the first peak, at about 250 °C, practically does not exist. The

(34) *Handbook of Chemistry and Physics*, 67th ed.; CRC Press: Boca Raton, FL, 1986.

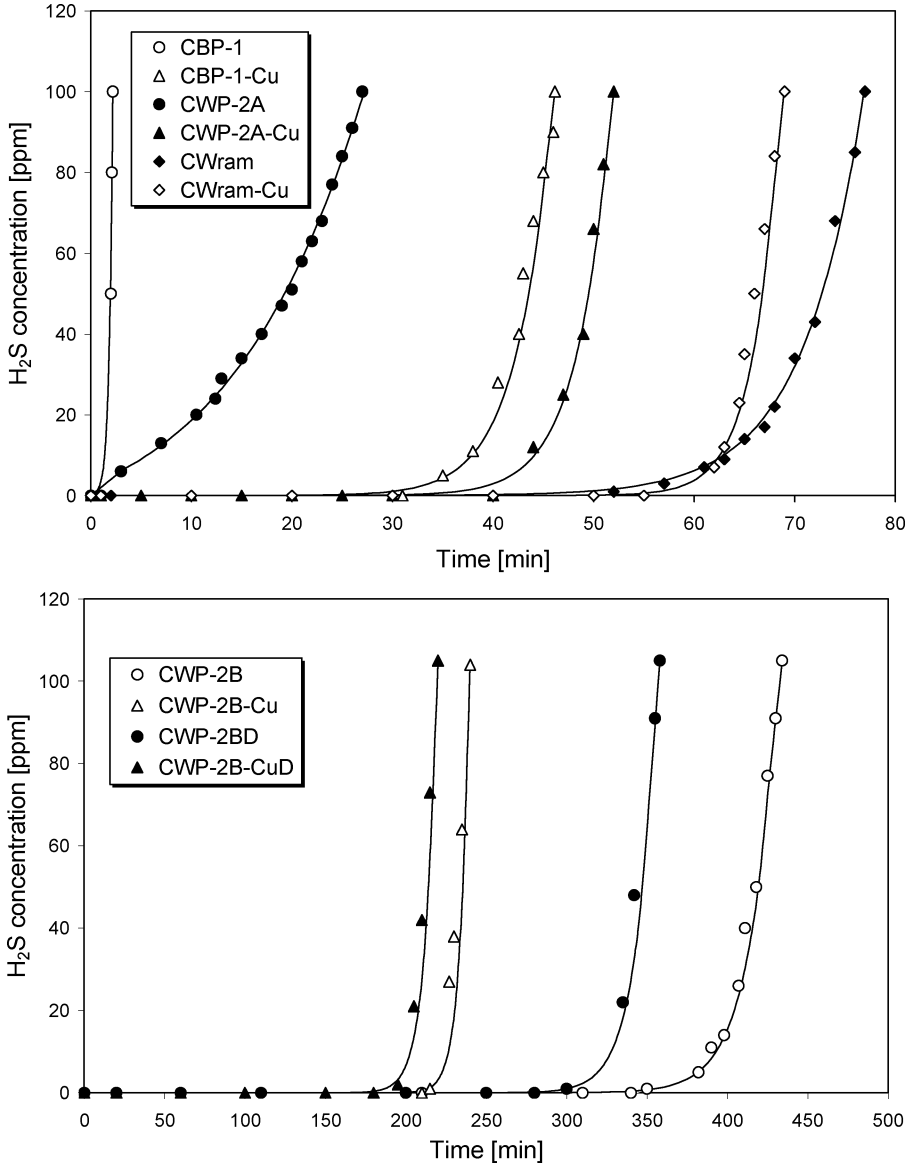

Figure 4. H_2S breakthrough capacity curves.

larger particle size significantly reduces surface area and therefore polymer loading and this in combination with more rapid diffusion through the sample reduces the intensity of this first peak. On the other hand, addition of copper results in an increase in the mass loss at 250 °C, which may be related to the decomposition of copper ion−organic phase complexes and its catalytic effect on graphitization. In this composite, the amine groups are about 70% modified with acetate groups. It is likely that the first stage of decomposition is decarboxylation of the modified amine sites and this could explain the absence of the first nitrogen loss peak (vide infra).

Although in all cases copper incorporation increases the yield of the materials (Table 2A), which might be the result of its presence and how it affects composite stability, in the case of CWP-2BCu, an exceptionally high (13%) increase in the weight was found that is in agreement with the data presented in Figure 2B. Indeed, comparison of the increases in the yield observed with an increase in the copper content (Table 2) reveals the same trend for all samples but CWP-2BCu, for which the effect of copper on the organic phase must be different. Here, the initial decomposition phase may again be decarboxylation and thus nitrogen retention in cooperation with the chelation effect could account for this increased yield.

The mentioned effects are also seen via analysis of carbon, hydrogen, and nitrogen contents in our samples presented in Table 2. It is interesting that the highest carbon content was found for CWram and the lowest for CWP-2B. That small amount of carbon present in the latter sample is the result of lower polymer loading due to the lower surface area on the larger particle silica gel. The high content of carbon in CWram can be linked to the coexistence of pyridine with the linear polymer (Figure 1).[31] Addition of copper increases the carbon content only for sample CBP-1. This is consistent with DTG analysis, where a decrease in the intensity of the peak about 450 °C was observed for the sample exposed to copper adsorption (Figure 2A). It is interesting that for all samples but CBP-1 and CBP-1Cu, the ratio of the content of nitrogen to carbon is over 0.1.

The conclusions from analysis of the DTG data are also supported by a comparison of the elemental analysis before and after pyrolysis (Table 2b). The carbon content of all the

Table 3. Breakthrough Capacity, Amount of Water Adsorbed, and pH Values of the Carbon Surfaces

sample	H_2S breakthrough capacity (mg/g)	H_2S breakthrough capacity (mg/cm^3)	water adsorbed (mg/g)	pH	pHE
CBP-1	2	0.7	37	5.6	5.0
CBP-1-Cu	40	16	40	5.3	4.8
CWP-2A	20	9	53	7.3	6.0
CWP-2A-Cu	38	18	59	5.8	5.3
CWP-2B	307	170	126	10.2	8.6
CWP-2B-Cu	165	91	82	9.8	8.1
CWP-2BD	240	135	N.D.	10.2	8.4
CWP-2B-CuD	153	83	N.D.	9.8	8.0
CWram	54	27	49	7.5	4.2
Cwram-Cu	51	24	67	6.1	5.3

composites is dramatically reduced except for CuWRAM, where the presence of the aromatic system can nucleate the formation of graphene layers (vide infra). Nitrogen loss is also much lower for CuWRAM relative to the other composites undoubtedly due to the fact that the pyridinyl nitrogen is not lost during pyrolysis. Indeed, the N:C ratio is reduced by almost exactly one-half. This is consistent with the preferential loss of the aliphatic amines. The lower polymer loading of the larger particle size WP-2B is evident from its elemental analysis relative to WP-2A. Even more important is the much higher N/C ratios for WP-2A and WP-2B relative to BP-1 after pyrolysis, whereas this ratio is almost the same prior to pyrolysis (Table 2). This lends credence to the loss of carbon dioxide as the primary mechanism of decomposition for WP-2A and WP-2B, whereas for BP-1, aliphatic amine loss is the primary decomposition pathway.

Another important asset of these materials for desulphurization is the stability of the carbon layer. Because it was obtained at 600 °C in an inert atmosphere, the stability should be preserved up to this temperature. The situation might change in the presence of air or other oxidants. Figure 3 shows DTA curves obtained in air where the peaks represent the extent of the exothermic effects. In all cases, adding copper catalyzes ignition because the temperature of the exotherm decreases and that decrease is up to 100 °C. Overall, the silica−nitrogen-containing carbon composites burn at about 500 °C, which is slightly higher than for the average activated carbon.[35]

The features described above, in addition to porosity, should affect the performance of the materials as hydrogen sulfide removal media. The H_2S breakthrough capacity curves indicate that the materials differ and the best adsorbents are CWP-2B and CWP-2BCu (Figure 4). Although their performance depends on the presence of water in the gas phase, even with dry air, the capacity is higher than those for other adsorbents. The breakthrough capacity values calculated at 100 ppm H_2S in the outlet gas are collected in Table 3, along with the amount of water adsorbed during the pre-humidification and the surface pH before and after hydrogen sulfide adsorption. As expected, the H_2S breakthrough capacity on our samples is related to the surface hydrophilicity and pH. Although in the case of water a linear

(35) Van Der Merwe, M.; Bandosz, T. J. *J. Colloid Interface Sci.* **2005**, *282*, 102.

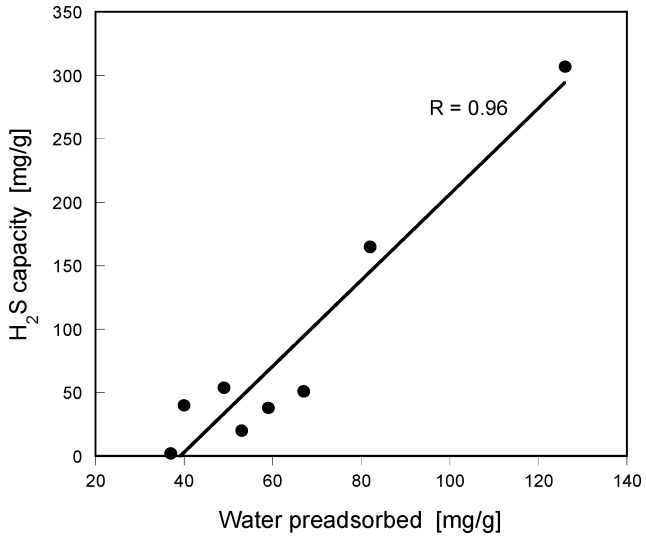

Figure 5. Dependence of the H_2S breakthrough capacity on the amount of water preadsorbed.

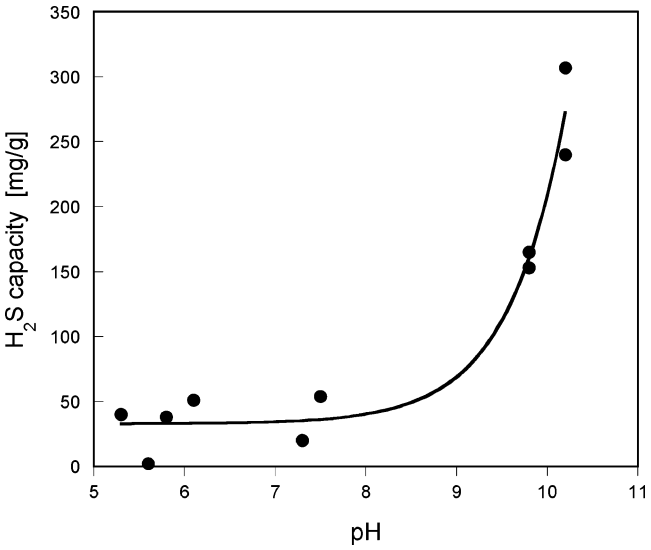

Figure 6. Dependence of the H_2S breakthrough capacity on the surface pH of adsorbents.

relationship between the capacity and the amount of water adsorbed is found (Figure 5), in the case of capacity/pH dependence (Figure 6) an indication of a threshold at the pH 9 is revealed. This must be related to formation of HS^- when surface chemistry allows it (the pH is greater than apparent pK_{a1} of hydrogen sulfide in the pore system).

The extent of surface hydrophilicity, assuming that carbon layer covers the pores of silica, is linked to the presence of nitrogen- and oxygen-containing functional groups.[13] The more heteroatoms that are incorporated into the carbonized silica surface as functional groups, the higher the water adsorption is. The surface pH value is also governed by those functional groups (if they have a distinct acidity or basicity) and the most basic ones are found on CWP-2B in spite of its low carbon content. This is consistent with the proposed decarboxylation, which occurs and leaves more nitrogen atoms as amines (vide supra) The most acidic surface is that of CBP-1, which in fact has the lowest H_2S removal capacity. As described elsewhere,[1] basic pH in the presence of water results in a shift in dissociation of hydrogen sulfide to the right and thus the oxidation efficiency of HS^- by oxygen

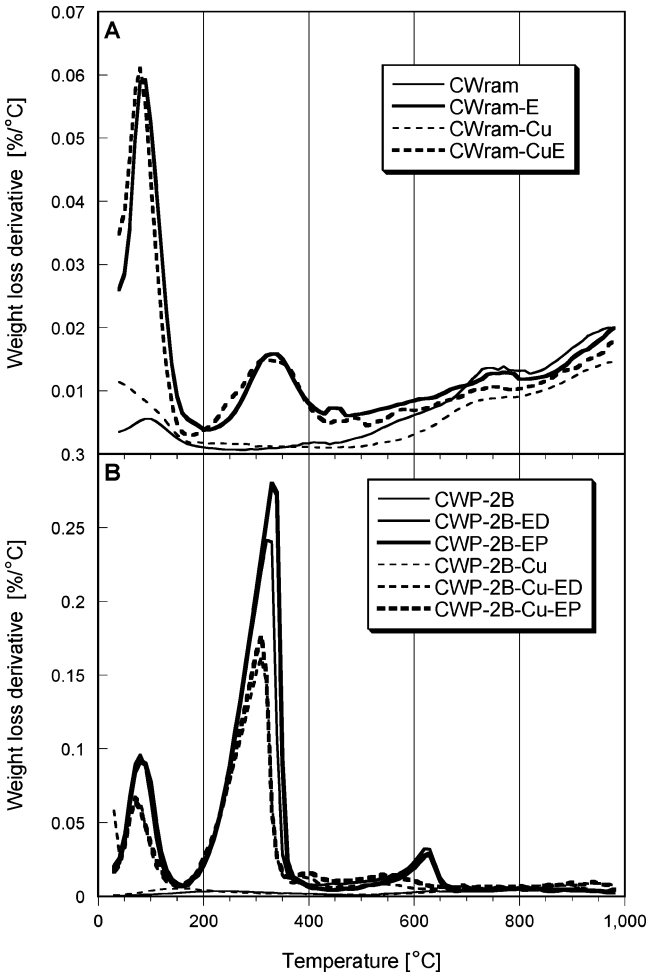

Figure 7. DTG curves in nitrogen for CWram series of samples (A) and CWP-2B series of samples (B) before and after H_2S adsorption.

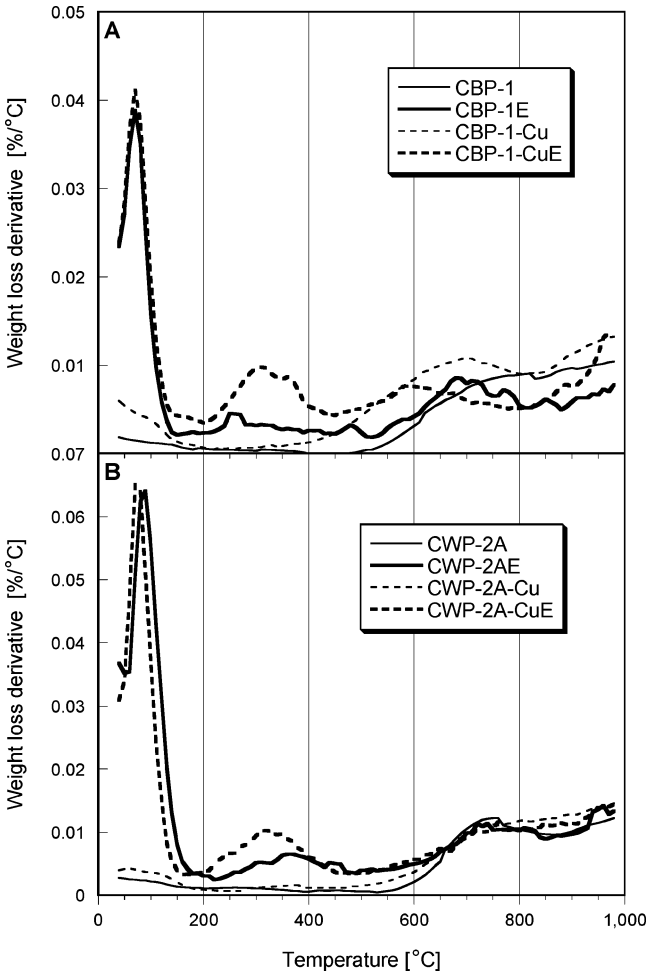

Figure 8. DTG curves in nitrogen for CBP-1 series of samples (A) and CWP-2A series of samples (B) before and after H_2S adsorption.

increases.[1] It is interesting that when the samples were not pre-humidified, their capacity was only 20% less compared to the situation when pre-humidification was applied. These results differ from those found for activated carbons. For them, the pre-humidification step was much more important.[1] This must be related to the kinetics of water adsorption and formation of water film. In the case of silica, the bigger pores help in establishing the surface layer of water in the small pores, whereas in the case of activated carbon, this process is usually very slow because of the much smaller pore sizes.[37]

Addition of copper to the system has a positive effect on the H_2S breakthrough capacities of the CBP-1Cu and CWP-2ACu samples. On the other hand, the capacities of CWP-2BCu and CWram-Cu, however high, were found to decrease after this kind of modifications. It is worth mentioning that for these two sorbents, similarities in the N:C ratio were found (Table 2). This suggests that in this particular case, complexation of copper blocks the active nitrogen species, which have their origin in the presence of pyridine or tertiary amines in the carbon precursor. For the samples in which copper significantly enhanced the removal capacity, the basicity of the nitrogen-containing groups was not enough to enhance the dissociation of hydrogen sulfide or active oxygen. Copper added to the system activated oxygen,[38,39] which resulted in a capacity on the level of about 30−50 mg/g, which was similar for all samples but CWP-2B, whose behavior as hydrogen sulfide removal media is exceptionally good.

The CWP-2B sample has a high hydrogen sulfide removal capacity in spite of its low carbon content. As seen from Table 3, adsorption of large quantities of hydrogen sulfide (almost 30 wt %) results in only a less than 2 pH units decrease in the surface pH. The fact that the surface remains basic suggests oxidation of hydrogen sulfide to elemental sulfur, which was the case for carbon modified with melamine[27] but not for carbon modified with urea, for which sulfuric acid was the main oxidation product.[23]

In Figures 7 and 8, DTG curves in nitrogen are presented. Peaks on the curves represent the mass loss as a result of removal/decomposition of surface oxidation products. Because our materials were obtained at 600 °C, only the features

(36) Brennan, J. K.; Bandosz, T. J.; Thomson, K. M.; Gubbins, K. *Colloid Surf., A* **2001**, *539*, 187−188.
(37) Harding, A. W.; Foley, N. J.; Norman, P. R.; Francis, D. C.; Thomas, K. M. *Langmuir* **1998**, *14*, 3858.
(38) Hafen, J. A.; Mahapatra, S.; Wilkinson, E. C.; Kaderli, S.; Young, V., Jr.; Que, L., Jr.; Zuberbuhler, A. D.; Tolman, W. B. *Science* **1996**, *272*, 1397.
(39) Hu, Z.; Williams, R. D.; Tran, D.; Spiro, T.; Gorun, S. *J. Am. Chem. Soc.* **2000**, *122*, 3556.
(40) Silverstein, R. M.; Bassler, G. C.; Morrill, T. C. *Spectroscopic Identification of Organic Compounds*; John Wiley and Sons: New York, 1981.

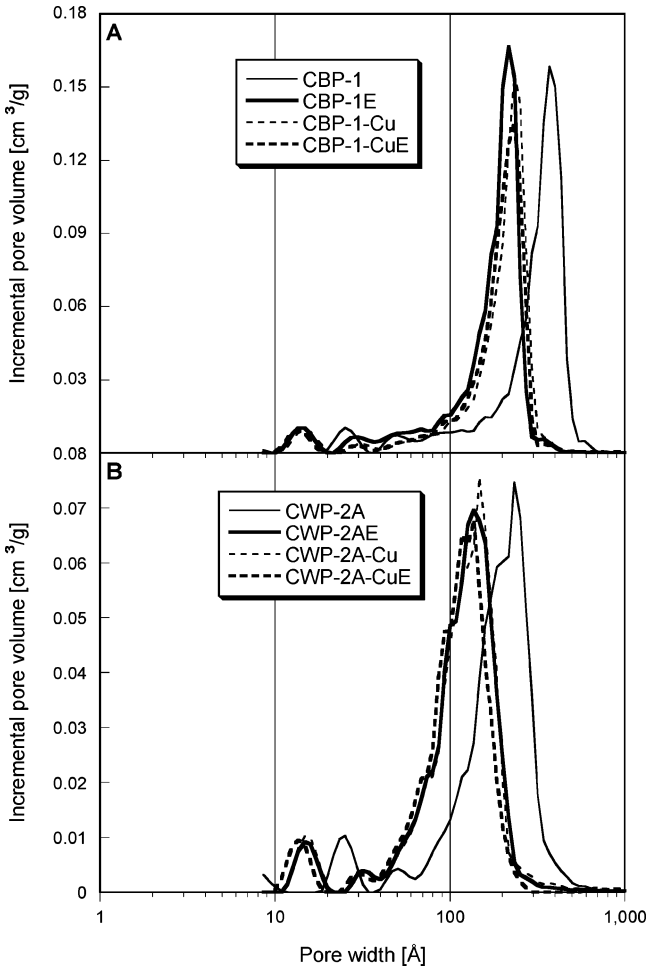

Figure 9. Pore size distributions for CBP-1 series of samples (A) and CWP-2A series of samples (B) before and after H_2S adsorption.

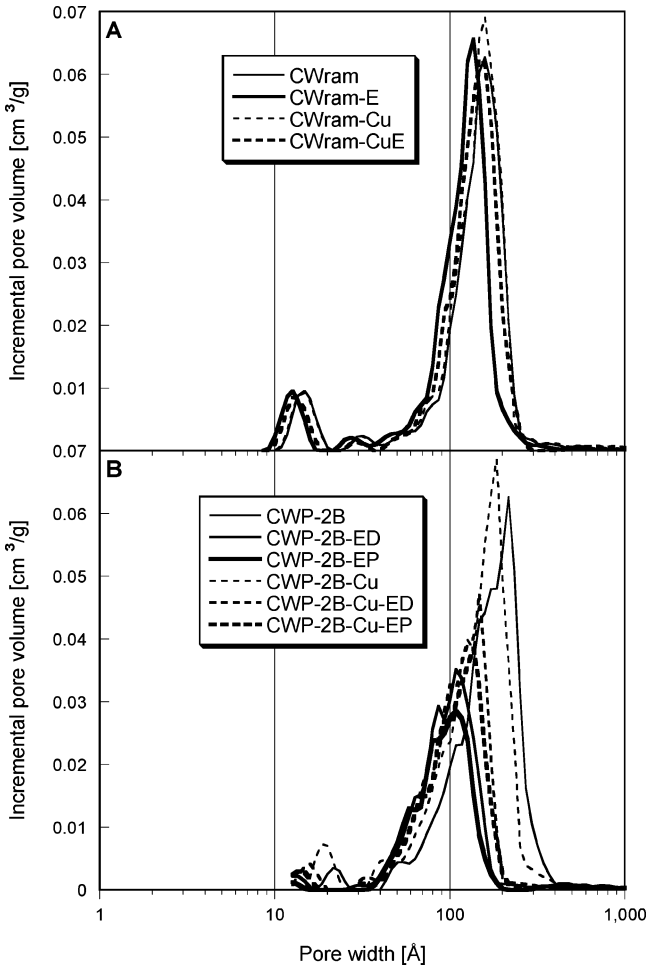

Figure 10. Pore size distributions for CWram series of samples (A) and CWP-2B series of samples (B) before and after H_2S adsorption.

at T < 600 °C can be discussed. The first peak, similar for all samples at about 100 °C, represents loss of water and weakly adsorbed SO_2. The second peak, between 200 and 500 °C is assigned to the removal of elemental sulfur. Its width is related the distribution of the pore sizes of the adsorbents. As shown previously,[29,30] sulfur from larger pores is removed at lower temperature. The order in intensity of this peak reflects the order in the values of the breakthrough capacity of the adsorbents studied. To confirm our assumption, the mass balance of sulfur present on the surface of CWP-2BE is presented in Table 4. Even though the data is not corrected for the mass loss of the samples not exposed to H_2S (as seen form Figure 7 and 8, the mass loss at T < 600 °C is minimal), a good agreement in the sulfur mass balance numbers indicates that almost all (about 90%) hydrogen sulfide is converted to elemental sulfur. That sulfur can be easily removed by heating at T < 400 °C or even at 120 °C if a vacuum is applied (during sample outgassing for porosity measurements, the condensation of elemental sulfur on the walls of the sample tube was noticed).

The elemental sulfur must be stored in the pore system of the adsorbents. The values of the structural parameters calculated from nitrogen adsorption isotherms are presented in Table 5. The surface areas are 200−450 m^2/g, which is typical for mesoporous silicas. In fact, the microporosity degree (V_{mic}/V_{mes}) being only between 10 and 20% clearly shows that the materials studied have the mesoporous

Table 4. Comparison of TA Mass Loss and Amount of Sulfur Adsorbed on the Basis of H_2S Breakthrough Experiments

sample	S−H_2S (wt %)	mass loss 200−500 °C (%)
CWP-2 BE	28.9	23.7
CWP-2 BED	22.6	20.9
CWP-2 BCuE	15.5	16.1
CWP-2 BCuED	14.4	14.8

structure with some fraction of micropores. Those pores seem to be the most active in the removal of hydrogen sulfide. For exhausted samples, especially those, which have the high capacity, the volume of micropores decreased 50% after hydrogen sulfide reactive adsorption. It has to mentioned here that that decrease in the volume of pores due to deposition of sulfur is underestimated because some sulfur was removed from the samples during outgassing. For CWP-2B, a decrease in the volume of mesopores after H_2S adsorption is also noticed, suggesting the contribution of their surface to the removal process and deposition of elemental sulfur there. In fact, to store 30 wt % sulfur, a significant volume of pores is needed. Incorporation of copper does not affect the porosity in a noticeable way. For all samples, the parameters of porous structure decreased after exposure to H_2S.

More details on the porous structure can be obtained from the analysis of pore size distributions presented in Figures 9 and 10. Although all samples have similar distributions with one large peak between 100 and 300 Å indicating the mesoporous structure, the differences in the sizes of small

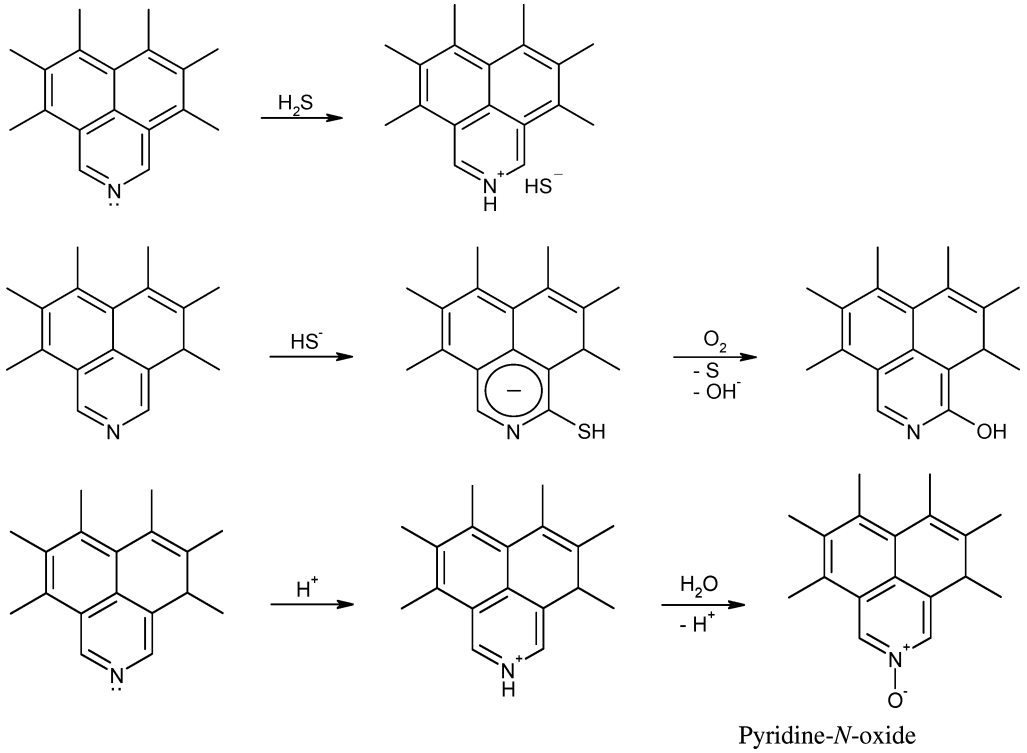

Figure 11. Possible surface reaction paths. The condensed aromatic rings represent the fragments of graphene layers.

Table 5. Structural Parameters Calculated from Adsorption of Nitrogen at −196 °C

sample	S_{BET} (m^2/g)	V_{mic} (cm^3/g)	V_{mes} (cm^3/g)	V_t (cm^3/g)	V_{mic}/V_t (%)
CBP-1	395	0.140	1.106	1.106	11
CBP-1E	378	0.135	1.084	1.219	11
CBP-1-Cu	334	0.127	0.966	1.093	12
CBP-1-CuE	290	0.110	0.936	1.046	11
CWP-2A	448	0.170	0.772	0.942	18
CWP-2AE	396	0.148	0.741	0.889	17
CWP-2A-Cu	412	0.157	0714	0.871	18
CW-2A-CuE	356	0.132	0.706	0.838	16
CWP-2B	261	0.093	0.586	0.679	14
CWP-2BE	112	0.047	0.285	0.332	14
CWP-2B-Cu	288	0.105	0.611	0.716	15
CWP-2B-CuE	149	0.059	0.361	0.420	14
CWP-2BD	135	0.055	0.0332	0.387	14
CWP-2B-CuD	186	0.072	0.421	0.493	15
CWram	305	0.126	0.512	0.638	20
CWram-E	228	0.091	0.479	0.570	16
CWram-Cu	322	0.133	0.543	0.676	20
CWram-CuE	246	0.099	0.521	0.620	16

pores and their accessibility are seen. Whereas for linear polymers the pores between 10 and 20 Å are revealed, for the branched ones, the very small pores do not exist suggesting the blocking of their entrances by carbon deposits after pyrolysis. Copper adsorption shifts the distribution to the left with the highest decrease in the size of pores for the CBP-1 and CWP-2A. This might be related to the differences in the fluid solid interactions used for PSD calculations and similarities in the loading of copper in these two samples. On the other hand, for the CWram and CWP-2B series of materials, the copper uptake does not have a visible effect on the pore size distribution. In the case of CWP-2B samples, a decrease in the intensity and size of pores is observed after exposure to hydrogen sulfide, which is in agreement with an increasing amount of sulfur deposited in the pores. That sulfur is deposited in small micropores (they practically disappear after H_2S adsorption) and pores larger than 200 Å. Pores of such sizes were also found to be important for adsorption of hydrogen sulfide on sludge-derived samples exposed to the catalytic surface.[29,30] Because no dependence of the capacity on the total pore volume was found, the performance of these composite samples is apparently governed by surface chemistry of the carbon phase.

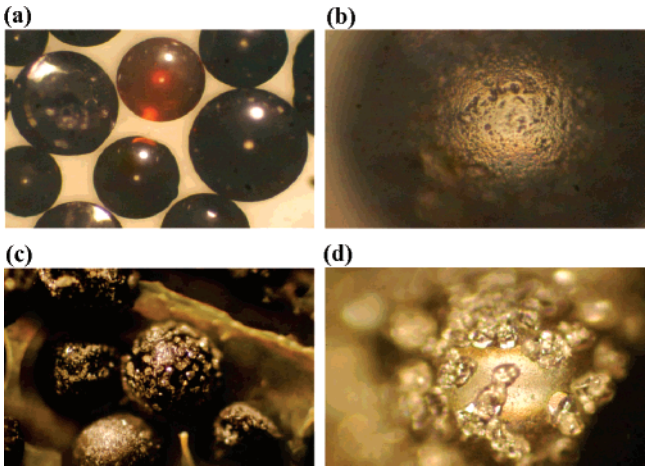

Figure 12. Optical microscopy images of the surface of the initial adsorbent, CWP-2B (A, B), and that exposed to H_2S reactive adsorption, CWP-2BE (C,D).

The possible reaction paths for adsorbents with basic pyridine-like compounds on the surface are presented in Figure 11. As seen, pyridine-like nitrogen is able to bind hydrogen sulfide even in its undissociated form; however, the compound formed is unstable. A more stable compound is formed when the sulfide ion is attached to the aromatic ring. This species is oxidized in the presence of oxygen and elemental sulfur and OH^- ions are the surface reaction products and the pyridine-like compound is converted to a pyridine phenol. On the other hand, H^+ ions in the presence

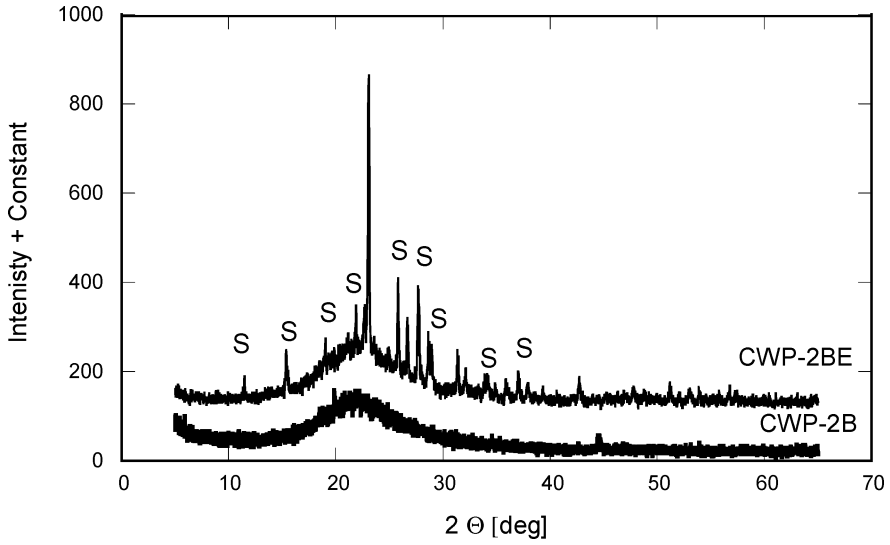

Figure 13. X-ray diffraction pattern for CWP-2B and CWP-2BE.

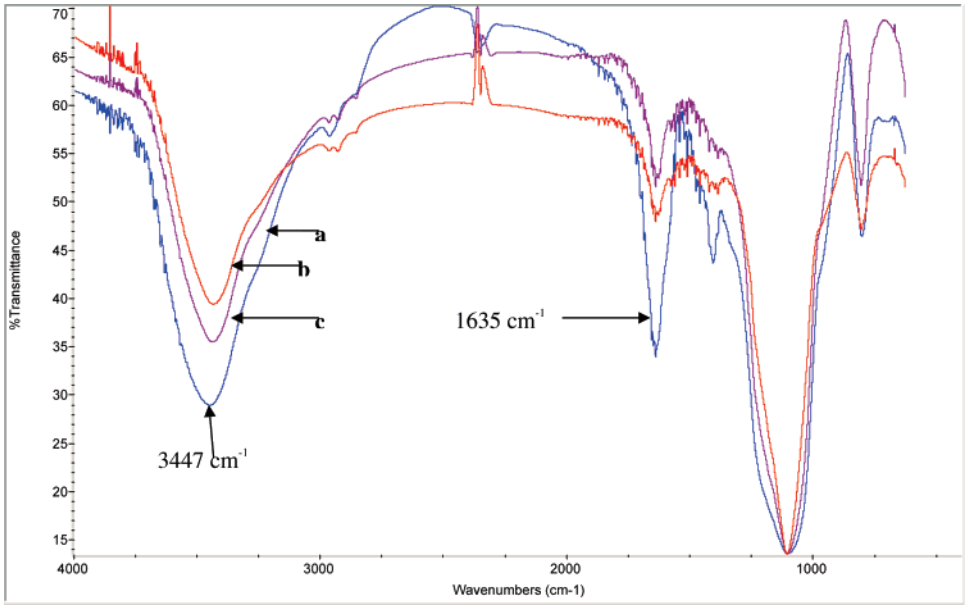

Figure 14. FT-IR of (a) WP-2B, (b) CWP-2B-Cu, (c) WP-2 EP-H2S-3000.

of water result in formation of pyridine *N*-oxide. These changes, along with the deposition of sulfur on the active sites, results in exhaustion of the adsorption capacity.

This deposition of sulfur in the crystalline form is seen on the surface of adsorbent particles (Figure 12). Images a and b of Figure 12 show the smooth surface of the silica spheres. The low carbon content in CW-2B sample causes the spheres to be translucent. After exposure to hydrogen sulfide the surface of the spheres is covered by crystals of sulfur of various sizes (images c and d of Figure 12). In fact, the sulfur present on the surface is in either the rhombohedral or monoclinic form, as seen on X-ray diffraction pattern presented in Figure 13.

The FT-IR and CPMAS ^{12}C NMR support the conclusions reached regarding the surface composition of the pyrolyzed composites. The FT-IR of WP-2B, WP-2B-Cu, and WP-2B-EP-H_2S samples show a much more intense band at 1635 cm^{-1} compared with those CuWram and BP-1 that can be assigned to the R−N−H bending (Figure 14). The intense band at 3447 cm^{-1} is assigned to an overlap between the N−H and OH stretches from the amines and from adsorbed moisture. Also notable is the appearance of weak C−H stretches above 3000 cm^{-1}, indicating the formation of aromatic moieties on the surface. The pyrolyzed samples of BP-1 and CuWRAM exhibit only very weak or no absorptions at 1635 cm^{-1}, and the intense peak at 3447 cm^{-1} shows diminished shouldering, indicating a decrease in the intensity of the N−H stretch for these samples typically observed at 3350 cm^{-1}. These assignments are consistent with the higher pH observed for the WP-2 samples and the DTG, both of which suggest that decarboxylation is a major pathway for the composites containing the amino acetate ligand.

The solid-state CPMAS ^{13}C NMR of WP-2A and WP-2B before and after pyrolysis lends further support to the conclusions drawn from the previous data. Prior to pyrolysis WP-2 exhibits a broad envelope of resonances centered at 44.5 ppm due to the polyamine carbons, a resonance at −10.3 ppm due to the silane methyls on the surface of the silica gel, and a resonance at 161.8 ppm due to the carboxylates (Figure 15a). After pyrolysis, a very broad ill defined

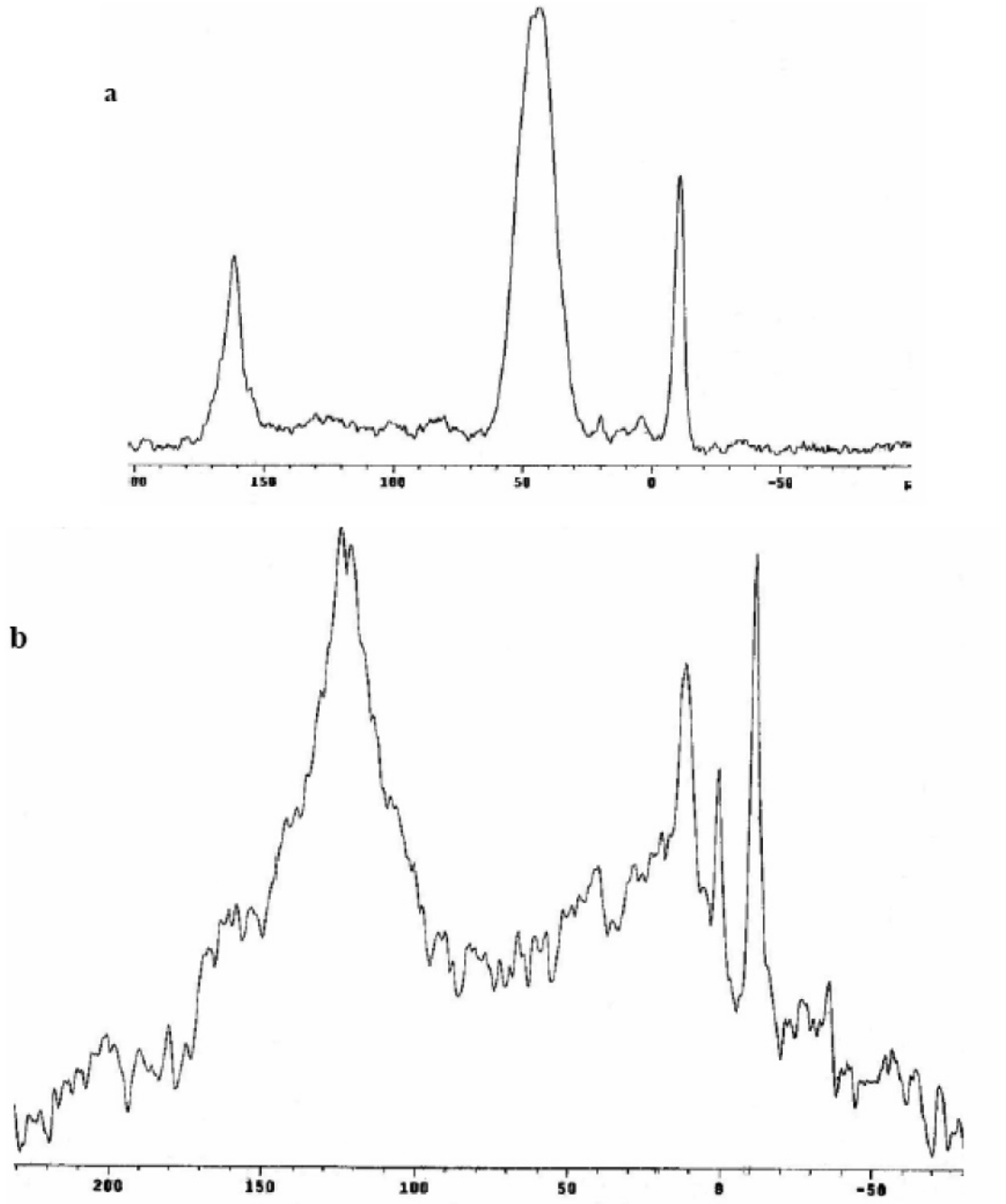

Figure 15. Solid-state CPMAS ^{13}C NMR of (a) WP-2B prior to pyrolysis, (b) WP-2B after pyrolysis.

spectrum is observed but with some interoperable changes. The aliphatic polymer resonances have diminished in intensity, as has the carboxylate peak at 161.8 ppm (Figure 15b). We assign a new broad envelope of resonances centered at 126.5 ppm to the formation of aromatic graphene type structures. The two peaks in the 0−20 ppm range are due to the silyl-propyl anchor (the third propyl peak is hidden in the broad resonances downfield). The methyl peak at −10.1 ppm is due to the silyl-methyl peak that arises from using a mixture of methyl trichlorosilane and chloropropyl trichlorosilane to coat the surface of the silica gel. This shows that the silanized surface has not been significantly decomposed during pyrolysis. The increase in their intensity is due to relative scaling. When the aliphatics are converted to graphene layers, the more cross-polarized remaining aliphatic peaks appear more intense because the quaternary carbons in the graphene layers are much less cross polarized.[31d] There is significant remaining signal intensity in the 40−50 ppm polyamine region. In contrast, pyrolyzed CuWRAM shows almost no intensity in the aliphatic region of the spectrum but shows very intense and relatively narrow (compared to WP-2) aromatic envelope resonances centered at 125.3 ppm. Thus, the decomposition pathway of WP-2 involves decarboxylation and graphene formation but where some of the polyamines remain on the surface resulting in a higher surface pH. The CuWRAM (and BP-1) decomposition pathways involve only graphene formation with loss of most if not all of the aliphatic amines and in the case of CuWRAM, graphene formation appears to be more efficient because of the initial presence of the aromatic pyridine moiety.

4. Conclusions

The results presented in this paper indicate the possibility of application of silica−carbon composites for the process of hydrogen sulfide adsorption/oxidation. Both the silica matrix and carbon phase contribute to the measured high capacity (up to 30 wt %). Although the former provides accessible pores without diffusion limitations, the latter contributes to specific surface chemistry. That chemistry, based on carbon and nitrogen, via basic pH and activation of oxygen leads to the high removal efficiency with elemental sulfur as the main surface oxidation product. In the cases where nitrogen-based chemistry is not able to provide sufficient surface pH, addition of copper contributes to formation of elemental sulfur in large quantities deposited in the pore system.

Acknowledgment. The authors are grateful to Dr. Christian Kloc of Bell Laboratories, Lucent Technologies, for help in receiving the optical microscopy images. Help of Dr. Volodymyr Tsyalkovsyy from Clemson University in deriving the surface reaction paths is appreciated. E.R. and J.A. acknowledge the Montana Board of Research and Commercialization Technology, the National Science Foundation, and Purity Systems for support.

CM062984I